PCCP

ARTICLE TYPE

Cite this: DOI: 10.1039/xxxxxxxxxx

Supporting Information

Cameron J. Mackie,*[a] Alessandra Candian,[a] Xinchuan Huang,[b] Elena Maltseva,[c] Annemieke Petrignani,[c] Jos Oomens,[d] Wybren Jan Buma,[c] Timothy J. Lee,[e] and Alexander G. G. M. Tielens[a]

Received Date
Accepted Date

DOI: 10.1039/xxxxxxxxxx

www.rsc.org/journalname

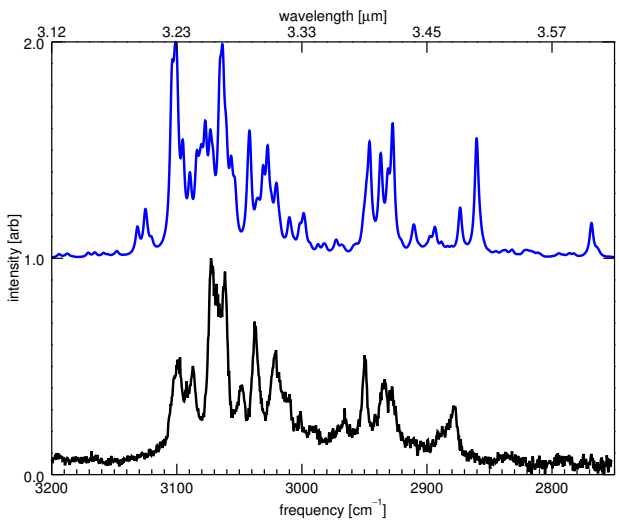

Fig. 1 Theoretical anharmonic IR spectrum of this work of 9–methylanthracene compared with the high–resolution gas–phase IR absorption spectrum of this work.

Table 1 Line positions [cm^{-1}], relative intensities, resonance components, and intensity origins for the bands of 9–methylanthracene determined from the high–resolution gas–phase IR absorption spectra and the theoretical anharmonic spectrum of this work (figure 1).

exp[1]	rel I[1]	anharm	rel I	components	I source
3099.3	0.53	3100.0	0.58	ν_2, $\nu_{13}+\nu_{22}$, ν_4	ν_2, ν_4
		3101.6	0.42	$\nu_{16}+\nu_{17}$, ν_{13}	ν_3
3092.3	0.43	3089.5	0.40	$\nu_{14}+\nu_{19}$, $\nu_{15}+\nu_{18}$, $\nu_{14}+\nu_{21}$, ν_8	ν_4, ν_1
3087.1	0.50	3083.8	0.50	$\nu_{13}+\nu_{19}$, ν_3	ν_3, ν_1
3072.7	1	3077.3	0.64	$\nu_{13}+\nu_{22}$, $\nu_{14}+\nu_{21}$, ν_1	ν_1, ν_4
3068.5	0.88	3073.1	0.60	$\nu_{14}+\nu_{22}$, $\nu_{14}+\nu_{19}$, $\nu_{13}+\nu_{22}$, ν_4	ν_4
3061.5	0.94	3063.6	0.99	ν_4, $\nu_{14}+\nu_{22}$, ν_5	ν_4, ν_3, ν_5, ν_6
3048.0	0.41	3056.6	0.47	ν_5, $\nu_{14}+\nu_{22}$	ν_5
3037.8	0.70	3041.8	0.26	ν_9, $\nu_{15}+\nu_{19}$, $\nu_{13}+\nu_{23}$, ν_5	ν_5, ν_9
		3041.6	0.32	$\nu_{16}+\nu_{18}$, ν_6	ν_6, ν_4
3020.6	0.58	3027.4	0.52	ν_{10}, $\nu_{15}+\nu_{21}$, $\nu_{15}+\nu_{22}$	ν_{10}
3001.2	0.30	2998.6	0.21	$\nu_{16}+\nu_{22}$, $\nu_{13}+\nu_{26}$	ν_4, ν_3
2965.8	0.30	2972.5	0.09	$\nu_{15}+\nu_{24}$	ν_4, ν_3
2949.8	0.55	2945.9	0.54	ν_{11}, $\nu_{18}+\nu_{20}$	ν_{11}
2933.8	0.44	2936.9	0.49	$\nu_{18}+\nu_{22}$, ν_{12}	ν_{12}
2927.9	0.40	2927.4	0.62	$\nu_{19}+\nu_{19}$, ν_{12}, $\nu_{18}+\nu_{22}$	ν_{12}
2877.5	0.32	2860.3	0.55	$\nu_{20}+\nu_{20}$, ν_{12}	ν_{12}

[a] *Leiden Observatory, Leiden University, PO Box 9513, 2300 RA Leiden, The Netherlands. E-mail: mackie@strw.leidenuniv.nl*
[b] *SETI Institute, 189 Bernardo Avenue, Suite 200, Mountain View, California 94043, United States.*
[c] *University of Amsterdam, Science Park 904, 1098 XH Amsterdam, The Netherlands.*
[d] *Radboud University, Toernooiveld 7, 6525 ED Nijmegen, The Netherlands.*
[e] *NASA Ames Research Center, Moffett Field, California 94035-1000, United States.*

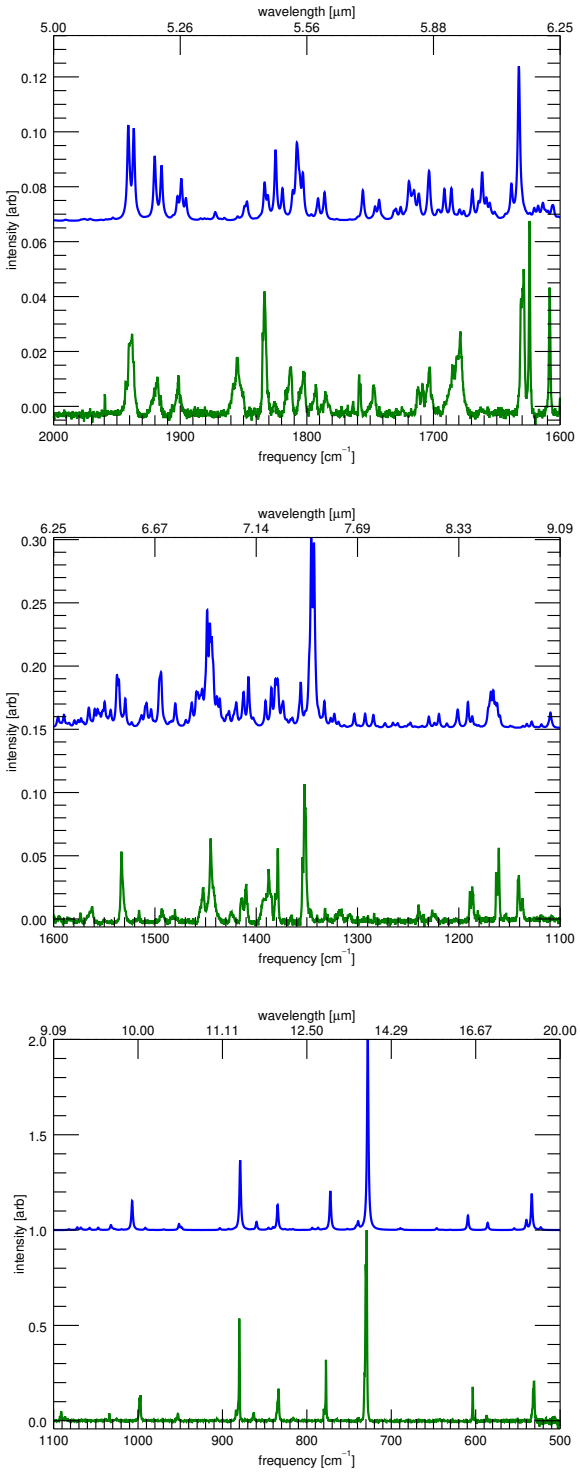

Fig. 2 The matrix–isolation infrared spectrum[2,3] of 9–methylanthracene (green, bottom of each panel) compared to the convolved (FWHM 2 cm^{-1}) theoretical anharmonic calculations of this work (blue, top each panel). Three spectral ranges are shown, with each range normalized to the local maximum to enhance details.

Table 2 Line positions [cm^{-1}], relative intensities, and vibrational mode identifications for the bands of 9–methylanthracene determined from the matrix isolation spectra and the theoretical anharmonic spectrum of this work (figure 2).

exp[2,3]	rel I	anharm	rel I	mode
1939.1	0.030	1941.0	0.035	$\nu_{42} + \nu_{42}$
1918.8	0.012	1920.2	0.024	$\nu_{44} + \nu_{42}$
1901.5	0.011	1899.1	0.015	$\nu_{45} + \nu_{44}$
1855.0	0.018	1847.3	0.007	$\nu_{47} + \nu_{43}$
1833.4	0.045	1824.7	0.026	$\nu_{42} + \nu_{49}$
1825.7	0.004	1819.3	0.012	$\nu_{43} + \nu_{49}$
1813.5	0.016	1807.9	0.029	$\nu_{46} + \nu_{46}$
1802.4	0.015	1803.2	0.018	$\nu_{45} + \nu_{49}$
1793.3	0.009	1791.1	0.008	$\nu_{45} + \nu_{50}$
1784.9	0.006	1786.0	0.010	$\nu_{44} + \nu_{50}$
1758.4	0.013	1755.8	0.011	$\nu_{47} + \nu_{47}$
1747.2	0.010	1742.9	0.008	$\nu_{43} + \nu_{52}$
1711.9	0.006	1719.4	0.014	$\nu_{48} + \nu_{48}$
1709.8	0.008	1715.4	0.011	$\nu_{47} + \nu_{50}$
1703.3	0.016	1703.5	0.018	$\nu_{44} + \nu_{53}$
1682.7	0.018	1669.3	0.011	$\nu_{37} + \nu_{58}$
1678.8	0.017	1661.6	0.018	$\nu_{45} + \nu_{55}$
1629.7	0.053	1632.7	0.056	ν_{13}
1573.4	0.007	1572.9	0.008	$\nu_{28} + \nu_{70}$
1563.0	0.010	1565.2	0.016	ν_{16}
1532.6	0.052	1537.4	0.042	ν_{17}
1515.6	0.009	1508.3	0.020	$\nu_{51} + \nu_{56}$
1492.9	0.008	1494.0	0.044	ν_{18}
1480.9	0.004	1479.9	0.020	$\nu_{54} + \nu_{54}$
1452.7	0.024	1457.7	0.028	$\nu_{37} + \nu_{66}$
1444.5	0.053	1448.4	0.093	$\nu_{44} + \nu_{63}$
1424.3	0.007	1419.7	0.020	$\nu_{45} + \nu_{64}$
1414.3	0.020	1412.4	0.029	$\nu_{47} + \nu_{61}$
1410.1	0.029	1407.6	0.041	ν_{23}
1388.2	0.023	1390.8	0.022	ν_{24}
1387.6	0.020	1385.1	0.032	ν_{25}
1378.8	0.056	1380.9	0.039	$\nu_{49} + \nu_{61}$
1352.1	0.104	1345.6	0.151	ν_{27}
1332.0	0.011	1332.7	0.021	ν_{28}
1317.5	0.007	1322.9	0.011	$\nu_{54} + \nu_{59}$
1307.9	0.005	1303.2	0.011	$\nu_{52} + \nu_{61}$
1239.5	0.011	1229.6	0.009	ν_{31}
1225.1	0.006	1219.6	0.011	$\nu_{58} + \nu_{58}$
1189.1	0.022	1191.0	0.021	ν_{32}
1186.6	0.026	1186.8	0.009	ν_{33}
1162.9	0.036	1168.3	0.029	$\nu_{52} + \nu_{66}$
1160.6	0.057	1166.0	0.030	ν_{34}
1141.0	0.039	-	-	
1137.3	0.017	-	-	
1090.9	0.049	1109.5	0.012	$\nu_{60} + \nu_{60}$
1086.5	0.017	-	-	
1033.9	0.041	1032.1	0.027	ν_{38}
997.8	0.133	1007.0	0.153	ν_{41}
952.8	0.038	951.5	0.032	ν_{44}
880.0	0.507	879.1	0.363	ν_{47}
863.1	0.041	859.6	0.043	ν_{48}
833.9	0.156	834.6	0.133	ν_{50}
816.1	0.016	816.7	0.006	$\nu_{62} + \nu_{69}$
777.4	0.301	772.2	0.205	ν_{52}
729.7	1	727.9	1	ν_{55}
603.5	0.175	609.2	0.076	ν_{58}
587.0	0.030	585.8	0.038	ν_{59}
531.3	0.217	533.6	0.191	ν_{61}

Table 3 Harmonic mode descriptions and frequencies [cm^{-1}] of the IR active modes and modes involved in IR active combination bands for the identifications given in tables 1 and 2 of 9–methylanthracene.

mode	freq	symm	description
ν_1	3225.9	a′	hindered quarto CH stretch
ν_2	3219.1	a′	unhindered quarto CH stretch
ν_3	3202.1	a′	hindered quarto CH stretch
ν_4	3201.4	a′	unhindered quarto CH stretch
ν_5	3186.9	a′	hindered quarto CH stretch
ν_6	3186.3	a′	unhindered quarto CH stretch
ν_7	3176.8	a′	solo/quarto CH stretch
ν_9	3171.2	a′	solo CH stretch
ν_{10}	3165.6	a′	methyl CH stretch
ν_{11}	3083.7	a″	methyl CH stretch
ν_{12}	3038.6	a′	methyl CH stretch
ν_{13}	1670.9	a′	CC stretch
ν_{14}	1664.2	a′	CC stretch
ν_{15}	1621.0	a′	CC stretch
ν_{16}	1601.1	a′	CC stretch
ν_{17}	1570.8	a′	CC stretch/CH in-plane bend
ν_{18}	1528.1	a′	CH in-plane bend
ν_{19}	1496.6	a′	methyl HCH bend
ν_{20}	1489.7	a″	methyl HCH bend
ν_{21}	1481.9	a′	CH in-plane bend
ν_{22}	1478.0	a′	CH in-plane bend
ν_{23}	1445.3	a′	CC stretch
ν_{24}	1420.1	a′	CH in-plane bend
ν_{25}	1413.1	a′	CH in-plane bend
ν_{26}	1408.6	a′	CH in-plane bend
ν_{27}	1373.8	a′	CH in-plane bend
ν_{28}	1356.7	a′	CH in-plane bend
ν_{31}	1252.0	a′	CH in-plane bend
ν_{32}	1210.4	a′	CH in-plane bend
ν_{33}	1200.7	a′	CH in-plane bend
ν_{34}	1181.4	a′	CH in-plane bend
ν_{37}	1078.8	a′	CH in-plane bend (incl. methyl)
ν_{38}	1050.6	a′	methyl CC stretch
ν_{41}	1025.1	a′	CH in-plane bend (incl. methyl)
ν_{42}	991.2	a″	CH out-of-plane bend
ν_{43}	989.2	a″	CH out-of-plane bend
ν_{44}	971.3	a″	CH out-of-plane bend
ν_{45}	967.3	a″	CH out-of-plane bend
ν_{46}	914.0	a′	CC in-plane bend
ν_{47}	898.6	a″	CH out-of-plane bend
ν_{48}	870.0	a′	CC in-plane bend
ν_{49}	860.2	a″	CH out-of-plane bend
ν_{50}	849.1	a″	CH out-of-plane bend
ν_{51}	830.6	a′	ring breathe
ν_{52}	785.8	a″	CC out-of-plane bend
ν_{53}	765.8	a″	CH out-of-plane bend
ν_{54}	747.2	a″	CH out-of-plane bend
ν_{55}	741.0	a″	CH out-of-plane bend
ν_{56}	698.2	a′	CC in-plane bend
ν_{58}	616.0	a′	CC in-plane bend
ν_{59}	600.8	a″	CC out-of-plane bend
ν_{60}	559.5	a′	CC in-plane bend
ν_{61}	544.8	a″	CC out-of-plane bend
ν_{62}	528.7	a′	CC in-plane bend
ν_{63}	506.8	a″	CC out-of-plane bend
ν_{64}	483.1	a″	CC out-of-plane bend
ν_{66}	405.2	a″	CC out-of-plane bend
ν_{69}	299.5	a″	CC out-of-plane bend
ν_{70}	248.3	a′	body in-plane bend

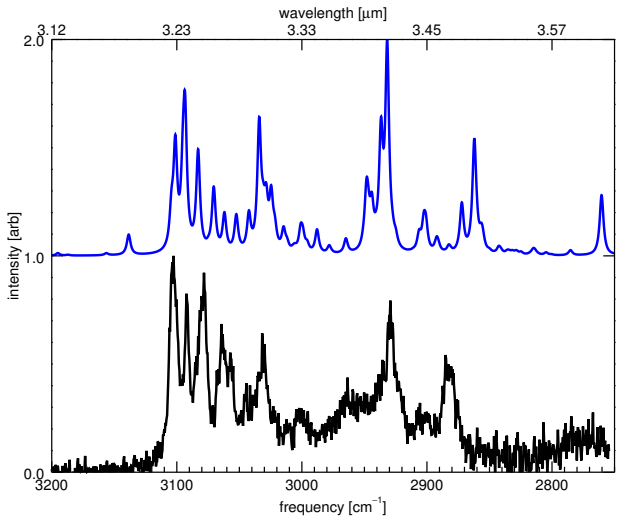

Fig. 3 Theoretical anharmonic IR spectrum of this work of 9,10–dimethylanthracene compared with the high–resolution gas–phase IR absorption spectrum of this work.

Table 4 Line positions [cm^{-1}], relative intensities, resonance components, and intensity origins for the bands of 9,10–dimethylanthracene determined from the high–resolution gas–phase IR absorption spectra and the theoretical anharmonic spectrum of this work (figure 3).

exp[1]	rel I[1]	anharm	rel I	components	I source
3102.6	1	3101.2	0.55	ν_4, $\nu_{16}+\nu_{25}$, $\nu_{16}+\nu_{21}$	ν_4
3092.3	0.83	3093.7	0.77	ν_2, $\nu_{19}+\nu_{20}$	ν_2
3078.3	0.92	3083.0	0.49	$\nu_{16}+\nu_{21}$, ν_4, ν_2	ν_4, ν_2
3063.7	0.47	3070.5	0.32	$\nu_{16}+\nu_{26}$, $\nu_{16}+\nu_{21}$, ν_5	ν_5
3057.3	0.55	3052.4	0.19	$\nu_{16}+\nu_{26}$, $\nu_{19}+\nu_{20}$, ν_5	ν_5
3031.7	0.64	3034.1	0.64	ν_9, $\nu_{15}+\nu_{27}$, $\nu_{18}+\nu_{21}$	ν_9, ν_4
2963.5	0.44	2964.8	0.08	$\nu_{20}+\nu_{21}$	ν_{14}
2929.2	0.79	2932.8	1	ν_{14}, $\nu_{21}+\nu_{24}$	ν_{14}
2885.2	0.54	2862.1	0.54	$\nu_{22}+\nu_{23}$, ν_{14}, $\nu_{21}+\nu_{24}$	ν_{14}

Table 5 Harmonic mode descriptions and frequencies [cm^{-1}] of the IR active modes and modes involved in IR active combination bands for the identifications given in table 4 of 9,10–dimethylanthracene.

mode	freq	symm	description
ν_2	3230.8	b	hindered quatro CH stretch
ν_4	3224.2	b	unhindered quatro CH stretch
ν_5	3196.9	b	CH stretch
ν_9	3168.7	b	methyl hindered CH stretch
ν_{14}	3038.3	b	methyl CH stretch
ν_{15}	1669.4	b	CC stretch
ν_{16}	1657.4	a	CC stretch
ν_{18}	1592.1	a	CC stretch
ν_{19}	1573.3	b	CC stretch
ν_{20}	1536.1	a	CH in-plane bend
ν_{21}	1507.1	b	methyl HCH bend
ν_{22}	1491.0	a	methyl HCH bend
ν_{23}	1490.8	a	methyl HCH bend
ν_{24}	1488.2	a	methyl HCH bend
ν_{25}	1482.5	b	CH in-plane bend
ν_{26}	1474.6	b	CH in-plane bend
ν_{27}	1450.5	a	CC stretch

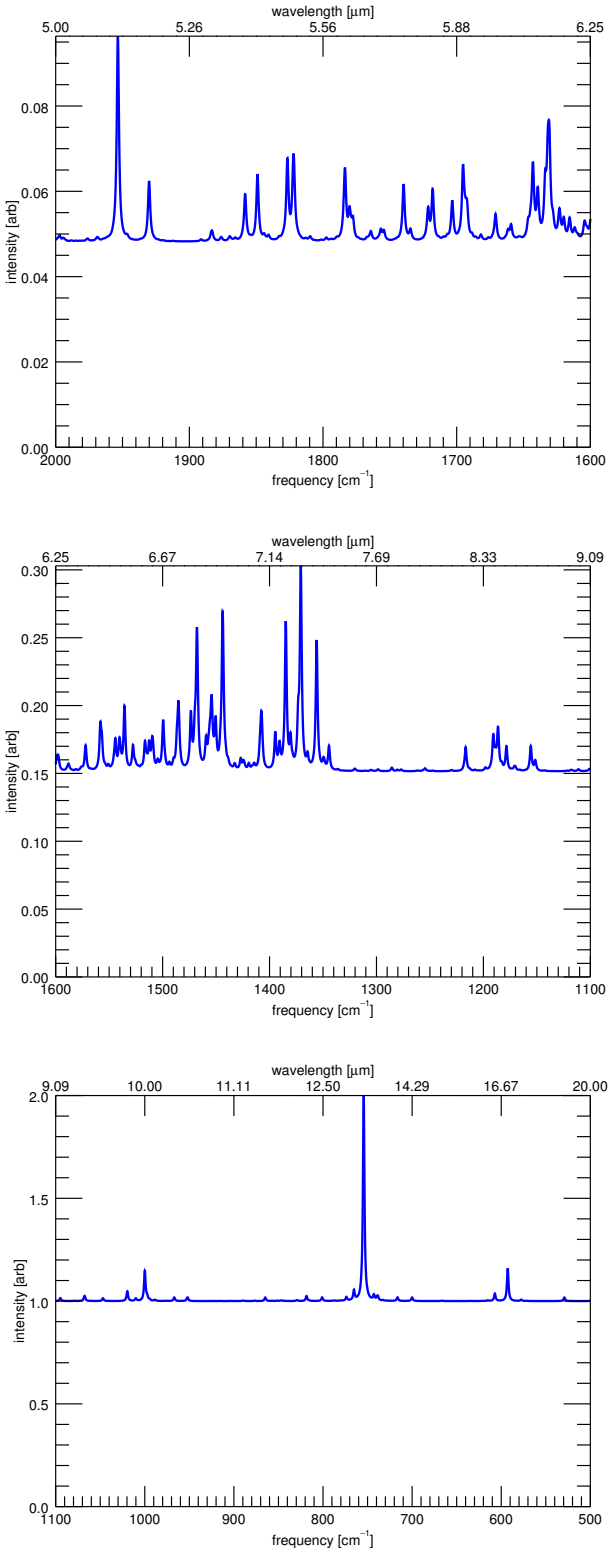

Fig. 4 No matrix–isolation data is available for 9,10–dimethylanthracene. Therefore, only the convolved (FWHM 2 cm^{-1}) theoretical anharmonic calculations of this work (blue, top each panel). Three spectral ranges are shown, with each range normalized to the local maximum to enhance details.

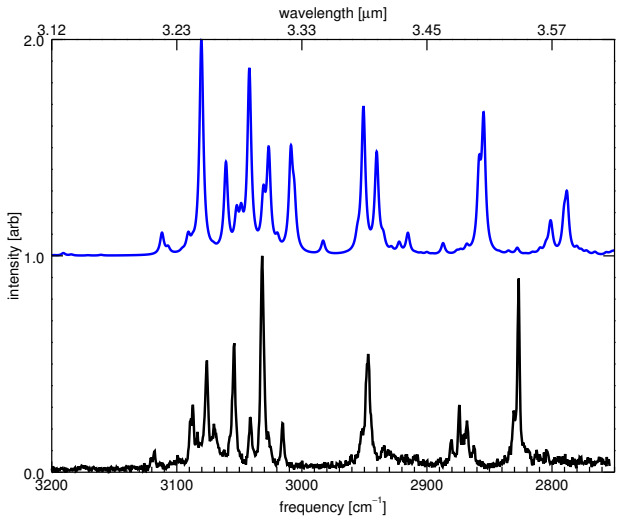

Fig. 5 Theoretical anharmonic IR spectrum of this work of 9,10–dihydroanthracene compared with the high–resolution gas–phase IR absorption spectrum of this work.

Table 6 Line positions [cm^{-1}], relative intensities, resonance components, and intensity origins for the bands of 9,10–dihydroanthracene determined from the high–resolution gas–phase IR absorption spectra and the theoretical anharmonic spectrum of this work (figure 5).

exp[1]	rel I[1]	anharm	rel I	components	I source
3118.1	0.10	3111.8	0.11	$\nu_{13}+\nu_{17}$	ν_7
3087.1	0.31	3090.7	0.11	$\nu_{14}+\nu_{18}$	ν_7
3075.9	0.52	3080.3	1	ν_4, $\nu_{15}+\nu_{19}$, $\nu_{16}+\nu_{20}$	ν_4
3070.3	0.22	3060.7	0.43	$\nu_{16}+\nu_{18}$, ν_5, $\nu_{14}+\nu_{19}$	ν_5
3054.0	0.60	3042.0	0.87	ν_5, $\nu_{13}+\nu_{20}$, $\nu_{14}+\nu_{19}$	ν_5
3041.5	0.25	3030.6	0.33	$\nu_{13}+\nu_{21}$, ν_7, ν_3	ν_7
3031.7	1	3026.4	0.50	ν_8, ν_4, $\nu_{16}+\nu_{20}$	ν_4
3015.5	0.23	3008.7	0.51	ν_7, $\nu_{16}+\nu_{19}$, $\nu_{15}+\nu_{20}$	ν_7
2947.0	0.55	2950.8	0.69	ν_{10}, $\nu_{14}+\nu_{23}$	ν_{10}
2934.2	0.12	2940.2	0.48	ν_{10}, $\nu_{14}+\nu_{23}$, $\nu_{13}+\nu_{25}$	ν_{10}
2880.2	0.15	2887.1	0.06	$\nu_{13}+\nu_{26}$	ν_5
2873.8	0.31	2858.0	0.47	ν_{11}, $\nu_{21}+\nu_{22}$	ν_{11}, ν_{10}
2868.0	0.24	2854.7	0.66	ν_{12}, $\nu_{21}+\nu_{21}$	ν_{12}
2862.6	0.12				
2830.6	0.28	2801.1	0.16	$\nu_{15}+\nu_{29}$, $\nu_{19}+\nu_{24}$	ν_{12}
2826.6	0.90	2788.2	0.30	$\nu_{19}+\nu_{24}$, ν_{12}	ν_{12}

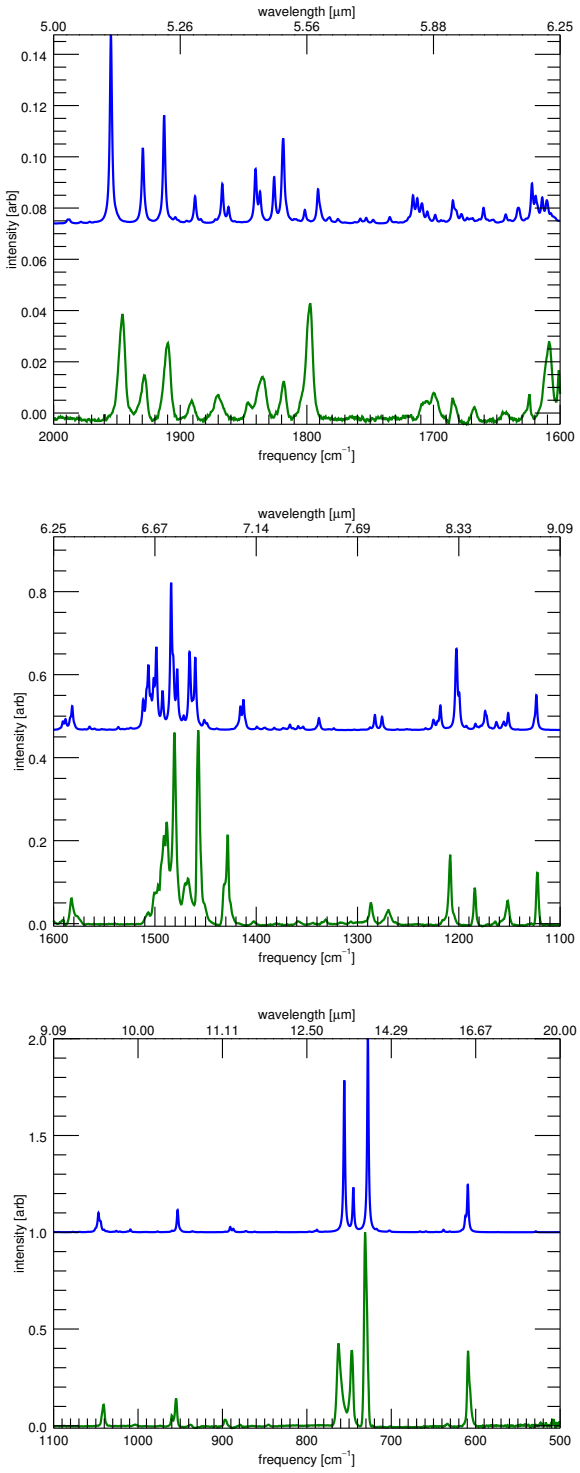

Fig. 6 The matrix–isolation infrared spectrum[2,3] of 9,10–dihydroanthracene (green, bottom of each panel) compared to the convolved (FWHM 2 cm^{-1}) theoretical anharmonic calculations of this work (blue, top each panel). Three spectral ranges are shown, with each range normalized to the local maximum to enhance details.

Table 7 Line positions [cm^{-1}], relative intensities, and vibrational mode identifications for the bands of 9,10–dihydroanthracene determined from the matrix isolation spectra and the theoretical anharmonic spectrum of this work (figure 6).

exp[2,3]	rel I	anharm	rel I	mode
1946.1	0.040	1954.7	0.074	$\nu_{42} + \nu_{41}$
1928.8	0.016	1929.5	0.030	$\nu_{44} + \nu_{41}$
1910.3	0.030	1912.7	0.042	$\nu_{45} + \nu_{42}$
1891.1	0.007	1888.3	0.011	$\nu_{45} + \nu_{44}$
1870.0	0.009	1866.8	0.016	$\nu_{46} + \nu_{41}$
1846.0	0.006	1840.5	0.021	$\nu_{49} + \nu_{41}$
1835.7	0.017	1837.0	0.013	$\nu_{47} + \nu_{44}$
1818.6	0.014	1825.8	0.018	$\nu_{46} + \nu_{45}$
1798.1	0.044	1818.7	0.033	$\nu_{45} + \nu_{48}$
1702.1	0.009	1709.1	0.008	$\nu_{41} + \nu_{55}$
1684.1	0.008	1684.7	0.009	$\nu_{45} + \nu_{52}$
1667.9	0.005	1660.5	0.006	$\nu_{45} + \nu_{54}$
1643.5	0.003	1643.0	0.004	$\nu_{47} + \nu_{52}$
1582.5	0.055	1581.7	0.058	ν_{16}
1507.5	0.025	1511.6	0.074	$\nu_{41} + \nu_{60}$
1499.7	0.069	1506.4	0.158	$\nu_{48} + \nu_{57}$
1489.5	0.228	1498.6	0.201	$\nu_{49} + \nu_{57}$
1480.6	0.418	1484.0	0.356	ν_{18}
1468.9	0.100	1478.0	0.148	$\nu_{53} + \nu_{54}$
1457.3	0.424	1465.8	0.189	$\nu_{43} + \nu_{61}$
1428.8	0.167	1412.6	0.074	ν_{22}
1402.5	0.006	1399.3	0.009	$\nu_{47} + \nu_{61}$
1358.4	0.006	1366.7	0.014	$\nu_{55} + \nu_{57}$
1331.8	0.009	1338.1	0.029	ν_{23}
1286.7	0.048	1282.9	0.037	ν_{26}
1269.8	0.031	1275.8	0.033	ν_{27}
1208.6	0.125	1202.3	0.196	ν_{30}
1184.2	0.089	1174.0	0.046	ν_{33}
1152.0	0.053	1151.3	0.041	ν_{34}
1122.4	0.129	1123.5	0.084	ν_{37}
1041.1	0.110	1046.9	0.101	ν_{39}
959.7	0.050	959.8	0.008	$\nu_{58} + \nu_{66}$
955.0	0.145	953.1	0.115	ν_{44}
937.9	0.006	935.7	0.005	ν_{45}
896.6	0.035	890.8	0.028	ν_{46}
761.6	0.387	755.7	0.784	ν_{52}
747.0	0.382	745.0	0.231	ν_{53}
730.5	1	727.7	1	ν_{54}
633.6	0.011	638.1	0.013	ν_{57}
608.5	0.351	609.3	0.246	ν_{58}

Table 8 Harmonic mode descriptions and frequencies [cm^{-1}] of the IR active modes and modes involved in IR active combination bands for the identifications given in tables 6 and 7 of 9,10–dihydroanthracene.

mode	freq	symm	description
ν_3	3202.6	b_2	quatro CH stretch
ν_4	3202.4	a_2	quatro CH stretch
ν_5	3188.3	a_1	quatro CH stretch
ν_7	3169.1	b_2	quatro CH stretch
ν_8	3168.8	a_2	dihydro CH in-plane stretch
ν_{10}	3077.3	b_2	dihydro CH in-plane stretch
ν_{11}	2984.6	b_2	dihydro CH out-of-plane stretch
ν_{12}	2979.9	a_1	dihydro CH out-of-plane stretch
ν_{13}	1654.8	b_2	CC stretch
ν_{14}	1647.5	a_2	CC stretch
ν_{15}	1633.8	a_1	CC stretch
ν_{16}	1620.0	b_1	CC stretch
ν_{17}	1528.6	a_1	CH in-plane bend
ν_{18}	1514.8	b_1	CH in-plane bend
ν_{19}	1491.9	a_2	CH in-plane bend
ν_{20}	1483.4	b_2	CH in-plane bend
ν_{21}	1471.1	a_1	dihydro HCH bend
ν_{22}	1466.1	b_2	dihydro HCH bend
ν_{23}	1373.6	a_2	CH in-plane bend
ν_{24}	1367.2	b_1	CH in-plane bend
ν_{25}	1351.8	a_1	CC stretch
ν_{26}	1307.2	b_2	CH in-plane bend
ν_{27}	1304.8	b_1	CH in-plane bend
ν_{29}	1234.1	a_1	CH in-plane bend
ν_{30}	1229.5	b_1	CH in-plane bend
ν_{33}	1195.3	b_2	CC in-plane bend
ν_{34}	1184.2	b_1	CH in-plane bend
ν_{37}	1141.1	b_2	CH in-plane bend
ν_{39}	1062.0	b_1	CC in-plane bend
ν_{41}	988.4	b_2	CH out-of-plane bend
ν_{42}	988.3	a_2	CH out-of-plane bend
ν_{43}	975.1	b_2	dihydro out-of-plane twist
ν_{44}	972.5	a_1	CH out-of-plane bend
ν_{45}	951.9	b_1	CH out-of-plane bend
ν_{46}	911.3	a_1	dihydro out-of-plane twist
ν_{47}	896.2	b_2	CH out-of-plane bend
ν_{48}	877.6	a_2	CH out-of-plane bend
ν_{49}	870.0	a_2	CC in-plane bend
ν_{52}	769.0	a_1	CC in-plane bend
ν_{53}	756.9	b_1	CH out-of-plane bend
ν_{54}	739.1	a_1	ring breathe
ν_{55}	726.3	a_2	CC out-of-plane bend
ν_{57}	641.9	b_2	CC out-of-plane bend
ν_{58}	618.8	a_1	CC in-plane bend
ν_{60}	530.9	a_2	CC in-plane bend
ν_{61}	521.2	a_2	CC out-of-plane bend
ν_{66}	359.0	a_1	body drum

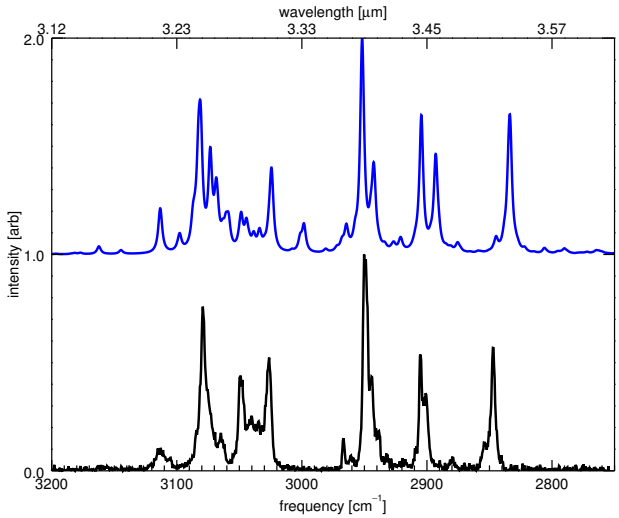

Fig. 7 Theoretical anharmonic IR spectrum of this work of 9,10–dihydrophenanthrene compared with the high–resolution gas–phase IR absorption spectrum of this work.

Table 9 Line positions [cm^{-1}], relative intensities, resonance components, and intensity origins for the bands of 9,10–dihydrophenanthrene determined from the high–resolution gas–phase IR absorption spectra and the theoretical anharmonic spectrum of this work (figure 7).

exp[1]	rel I[1]	anharm	rel I	components	I source
3112.9	0.10	3113.0	0.11	$\nu_{13}+\nu_{18}$, $\nu_{14}+\nu_{17}$, ν_1	ν_1
		3113.6	0.10	$\nu_{13}+\nu_{17}$, $\nu_{14}+\nu_{18}$, ν_4	ν_4
3079.2	0.76	3081.4	0.72	ν_2, $\nu_{16}+\nu_{18}$, ν_4	ν_2, ν_4
3064.7	0.18	3059.2	0.20	$\nu_{16}+\nu_{17}$, ν_1	ν_1
3048.9	0.44	3048.5	0.20	$\nu_{16}+\nu_{18}$, ν_2	ν_2
3040.1	0.25	3044.4	0.17	$\nu_{14}+\nu_{19}$, $\nu_{14}+\nu_{22}$	ν_4, ν_2
3034.5	0.23	3033.9	0.12	$\nu_{15}+\nu_{19}$, $\nu_{14}+\nu_{21}$, $\nu_{16}+\nu_{21}$, ν_5	ν_5
3026.2	0.52	3024.0	0.22	ν_7, $\nu_{15}+\nu_{22}$, $\nu_{14}+\nu_{21}$	ν_7
		3024.6	0.18	ν_8, $\nu_{13}+\nu_{21}$, ν_4	ν_4, ν_8
2966.7	0.15	2964.4	0.14	$\nu_{13}+\nu_{23}$, $\nu_{18}+\nu_{18}$	ν_9
2950.2	1	2951.8	1	ν_9	ν_9
2944.3	0.44	2942.6	0.43	ν_{10}, $\nu_{13}+\nu_{24}$, $\nu_{14}+\nu_{23}$	ν_{10}
2938.3	0.18	2941.8	0.14	$\nu_{15}+\nu_{23}$, $\nu_{14}+\nu_{24}$	ν_9
2905.1	0.54	2904.5	0.64	ν_{11}, $\nu_{20}+\nu_{22}$, ν_{10}	ν_{11}, ν_{10}
2901.0	0.36	2893.0	0.46	$\nu_{20}+\nu_{20}$, ν_{12}, ν_9	ν_9, ν_{12}
2879.7	0.07	2875.4	0.06	$\nu_{22}+\nu_{22}$, $\nu_{20}+\nu_{20}$	ν_{12}
2854.5	0.13	2845.6	0.07	$\nu_{17}+\nu_{23}$	ν_{11}
2847.2	0.57	2833.7	0.65	ν_{11}, $\nu_{20}+\nu_{22}$, $\nu_{17}+\nu_{23}$	ν_{11}

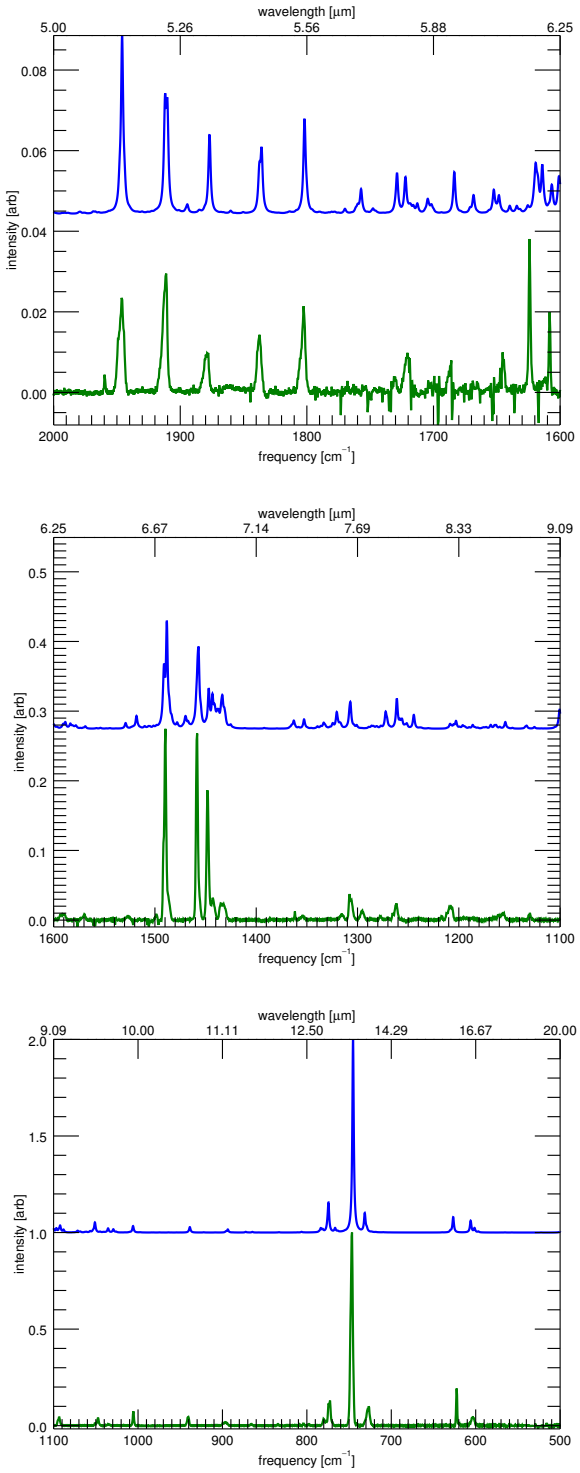

Fig. 8 The matrix–isolation infrared spectrum[2,3] of 9,10-dihydrophenanthrene (green, bottom of each panel) compared to the convolved (FWHM 2 cm^{-1}) theoretical anharmonic calculations of this work (blue, top each panel). Three spectral ranges are shown, with each range normalized to the local maximum to enhance details.

Table 10 Line positions [cm^{-1}], relative intensities, and vibrational mode identifications for the bands of 9,10–dihydrophenanthrene determined from the matrix isolation spectra and the theoretical anharmonic spectrum of this work (figure 8).

exp[2,3]	rel I	anharm	rel I	mode
1946.6	0.022	1945.9	0.044	$\nu_{44} + \nu_{43}$
1912.1	0.029	1910.3	0.029	$\nu_{45} + \nu_{44}$
1879.4	0.010	1876.8	0.020	$\nu_{46} + \nu_{45}$
1837.7	0.015	1835.8	0.017	$\nu_{48} + \nu_{44}$
1802.9	0.019	1801.8	0.024	$\nu_{48} + \nu_{46}$
1730.5	0.004	1728.8	0.010	$\nu_{49} + \nu_{48}$
1721.0	0.010	1722.1	0.009	$\nu_{51} + \nu_{46}$
1687.4	0.006	1683.6	0.010	$\nu_{54} + \nu_{45}$
1645.1	0.008	1648.3	0.005	$\nu_{51} + \nu_{49}$
1593.0	0.007	1590.5	0.007	$\nu_{37} + \nu_{61}$
1589.6	0.008	1588.5	0.010	ν_{15}
1569.9	0.007	1568.7	0.004	ν_{16}
1489.9	0.253	1488.2	0.154	ν_{18}
1458.5	0.276	1457.1	0.118	ν_{19}
1448.0	0.190	1446.9	0.058	ν_{21}
1443.1	0.030	1443.2	0.050	ν_{20}
1433.3	0.025	1433.5	0.049	ν_{22}
1361.9	0.012	1362.9	0.012	$\nu_{49} + \nu_{61}$
1354.4	0.005	1352.8	0.014	ν_{23}
1315.6	0.008	1320.5	0.024	$\nu_{38} + \nu_{68}$
1306.9	0.034	1307.1	0.039	ν_{26}
1295.4	0.013	-		
1277.4	0.006	1272.2	0.025	$\nu_{52} + \nu_{61}$
1262.0	0.022	1261.2	0.043	ν_{29}
1239.5	0.002	1244.4	0.020	$\nu_{51} + \nu_{62}$
1216.8	0.006	1208.6	0.007	$\nu_{53} + \nu_{63}$
1208.5	0.020	1202.8	0.011	ν_{30}
1165.4	0.004	1168.5	0.006	ν_{34}
1161.0	0.007	1163.3	0.006	$\nu_{52} + \nu_{66}$
1156.4	0.010	1154.1	0.010	ν_{35}
1130.1	0.008	1133.1	0.005	ν_{36}
1093.7	0.042	1092.3	0.037	ν_{37}
1047.5	0.038	1051.1	0.053	ν_{39}
1005.5	0.075	1005.9	0.034	ν_{41}
940.7	0.049	938.7	0.028	ν_{46}
896.9	0.017	893.7	0.016	ν_{47}
779.7	0.032	783.5	0.024	ν_{51}
773.3	0.132	774.4	0.156	ν_{52}
746.9	1	745.3	1	ν_{53}
727.4	0.095	731.4	0.102	ν_{55}
622.5	0.203	626.7	0.080	ν_{57}
603.5	0.044	606.0	0.062	ν_{58}

Table 11 Harmonic mode descriptions and frequencies [cm^{-1}] of the IR active modes and modes involved in IR active combination bands for the identifications given in tables 9 and 10 of 9,10–dihydrophenanthrene.

mode	freq	symm	description
ν_1	3208.4	a	quatro CH stretch
ν_2	3204.5	b	quatro CH stretch
ν_4	3193.8	b	quatro CH stretch
ν_5	3184.3	a	quatro CH stretch
ν_8	3170.5	b	quatro CH stretch
ν_9	3078.5	b	dihydro CH in-plane stretch
ν_{10}	3078.1	a	dihydro CH in-plane stretch
ν_{11}	3013.2	b	dihydro CH out-of-plane stretch
ν_{12}	3003.4	a	dihydro CH out-of-plane stretch
ν_{13}	1652.2	b	CC stretch
ν_{14}	1643.8	a	CC stretch
ν_{15}	1628.2	b	CC stretch
ν_{16}	1607.2	a	CC stretch
ν_{17}	1525.5	a	CH in-plane bend
ν_{18}	1519.1	b	CH in-plane bend
ν_{19}	1486.2	b	CH in-plane bend
ν_{20}	1481.6	a	dihydro HCH bend
ν_{21}	1472.8	b	dihydro HCH bend
ν_{22}	1472.6	a	CH in-plane bend
ν_{23}	1380.9	b	dihydro CH in-plane bend
ν_{24}	1369.1	a	CH in-plane bend
ν_{26}	1339.0	a	dihydro CH in-plane bend
ν_{29}	1282.1	a	CH in-plane bend
ν_{30}	1224.5	a	CH in-plane bend
ν_{34}	1182.1	b	quatro CH in-plane bend
ν_{35}	1178.0	b	dihydro CH in-plane bend
ν_{36}	1149.5	b	CH in-plane bend
ν_{37}	1110.2	a	CC in-plane bend
ν_{38}	1071.8	a	CC in-plane bend
ν_{39}	1068.8	b	CC in-plane bend
ν_{41}	1020.3	b	CC in-plane bend
ν_{43}	989.9	b	dihydro CC in-plane stretch
ν_{44}	988.1	a	CH out-of-plane bend
ν_{45}	955.7	a	CH out-of-plane bend
ν_{46}	955.6	b	CH out-of-plane bend
ν_{47}	908.0	b	dihydro out-of-plane twist
ν_{48}	879.7	b	CH out-of-plane bend
ν_{49}	878.8	a	CH out-of-plane bend
ν_{51}	791.8	a	CH out-of-plane bend
ν_{52}	782.7	b	CH out-of-plane bend
ν_{53}	757.1	b	CH out-of-plane bend
ν_{54}	737.0	a	CH out-of-plane bend
ν_{55}	734.7	b	CC out-of-plane bend
ν_{57}	633.1	b	CC in-plane bend
ν_{58}	610.0	b	CC out-of-plane bend
ν_{61}	503.7	b	CC out-of-plane bend
ν_{62}	470.5	a	CC out-of-plane bend
ν_{63}	466.6	b	CC out-of-plane bend
ν_{66}	392.1	a	body in-plane stretch
ν_{68}	268.2	a	body twist

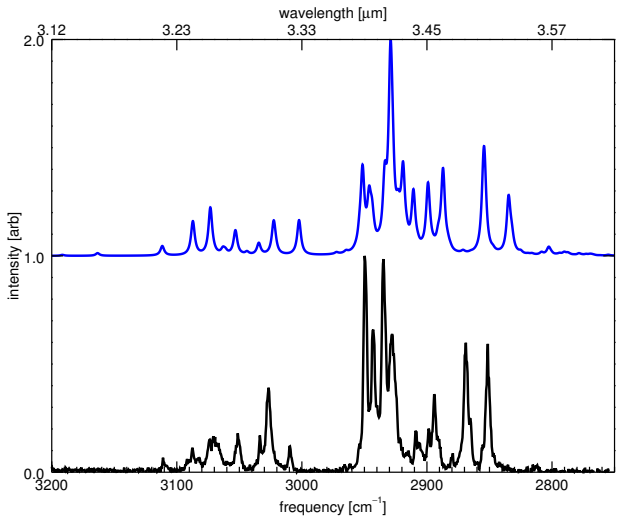

Fig. 9 Theoretical anharmonic IR spectrum of this work of 1,2,3,4–tetrahydronaphthalene compared with the high–resolution gas–phase IR absorption spectrum of this work.

Table 12 Line positions [cm^{-1}], relative intensities, resonance components, and intensity origins for the bands of 1,2,3,4–tetrahydronaphthalene determined from the high–resolution gas–phase IR absorption spectra and the theoretical anharmonic spectrum of this work (figure 9).

exp[1]	rel I[1]	anharm	rel I	components	I source
3111.0	0.07	3111.6	0.05	$\nu_{13}+\nu_{15}$, ν_4	ν_4
3087.6	0.10	3087.3	0.16	ν_1, $\nu_{14}+\nu_{15}$, $\nu_{13}+\nu_{18}$	ν_1
3082.5	0.07				
3073.6	0.15	3073.2	0.22	ν_2, $\nu_{14}+\nu_{18}$	ν_2
3070.8	0.17				
3051.2	0.18	3053.1	0.12	ν_3, ν_1, $\nu_{13}+\nu_{18}$	ν_1
3033.6	0.17	3034.4	0.06	ν_3, $\nu_{13}+\nu_{18}$, ν_1	ν_1
3026.6	0.39	3022.5	0.16	$\nu_{14}+\nu_{18}$, ν_4, ν_2	ν_4, ν_2
3009.5	0.12	3003.2	0.16	ν_4, $\nu_{14}+\nu_{18}$, ν_2	ν_4, ν_2
2949.8	1	2951.5	0.42	ν_6, $\nu_{16}+\nu_{16}$, $\nu_{17}+\nu_{17}$, ν_{10}	ν_6, ν_{10}
2942.9	0.66	2946.1	0.33	$\nu_{15}+\nu_{17}$, $\nu_{16}+\nu_{17}$, ν_9	ν_9, ν_8
2934.7	0.99	2929.0	1	ν_5	ν_5
2927.9	0.64	2919.1	0.44	$\nu_{16}+\nu_{16}$, ν_6	ν_6
2909.2	0.19	2910.8	0.31	$\nu_{17}+\nu_{17}$, ν_6, ν_{10}	ν_6, ν_{10}
2898.8	0.20	2899.1	0.34	$\nu_{16}+\nu_{19}$, ν_8	ν_8, ν_{12}
2894.2	0.36	2887.1	0.41	$\nu_{19}+\nu_{20}$, ν_{12}, ν_8, $\nu_{16}+\nu_{19}$	ν_{12}, ν_8
2879.3	0.09	2871.1	0.03	$\nu_{20}+\nu_{20}$, $\nu_{19}+\nu_{19}$	ν_{10}, ν_{11}
2868.9	0.60	2855.4	0.51	ν_{10}, $\nu_{17}+\nu_{17}$, $\nu_{16}+\nu_{20}$	ν_{10}
2851.3	0.60	2834.6	0.28	ν_{12}, $\nu_{19}+\nu_{20}$	ν_{12}

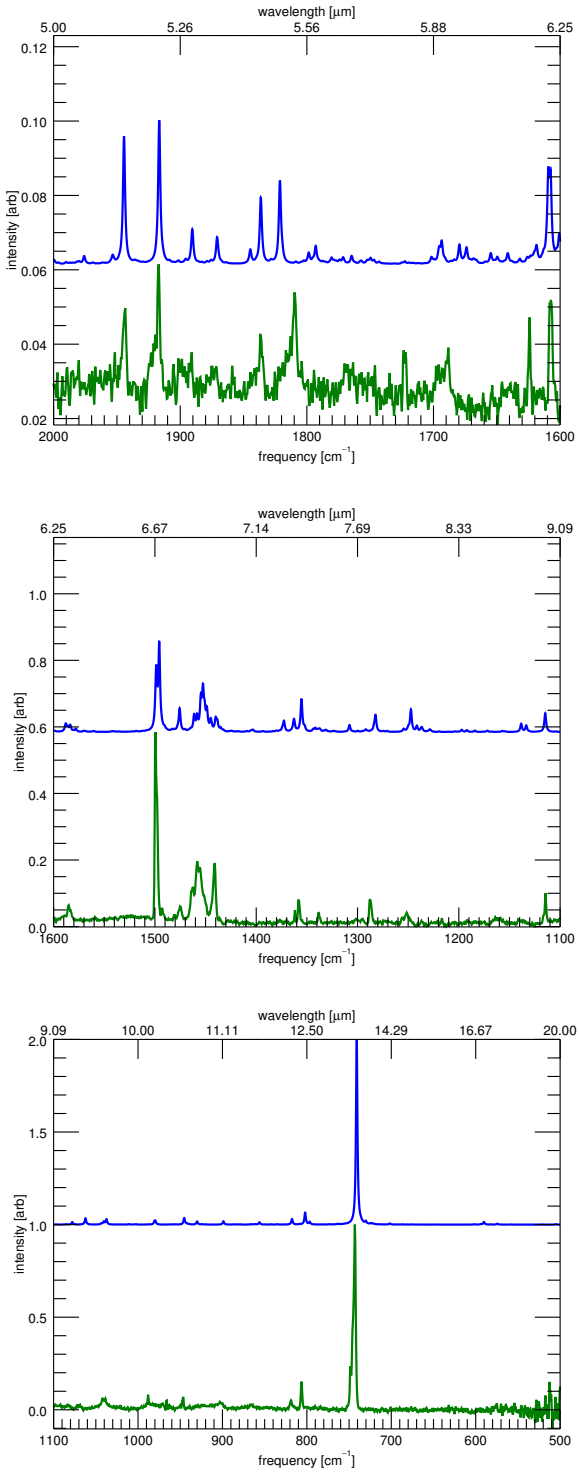

Fig. 10 The matrix–isolation infrared spectrum[2,3] of 1,2,3,4–tetrahydronaphthalene (green, bottom of each panel) compared to the convolved (FWHM 2 cm^{-1}) theoretical anharmonic calculations of this work (blue, top each panel). Three spectral ranges are shown, with each range normalized to the local maximum to enhance details.

Table 13 Line positions [cm^{-1}], relative intensities, and vibrational mode identifications for the bands of 1,2,3,4–tetrahydronaphthalene determined from the matrix isolation spectra and the theoretical anharmonic spectrum of this work (figure 10).

exp[2,3]	rel I	anharm	rel I	mode
1944.2	0.024	1944.4	0.034	$\nu_{39} + \nu_{39}$
1916.6	0.030	1916.6	0.039	$\nu_{40} + \nu_{39}$
1896.5	0.005	1890.5	0.009	$\nu_{40} + \nu_{40}$
1836.4	0.015	1837.4	0.011	$\nu_{27} + \nu_{30}$
1810.7	0.021	1821.3	0.023	$\nu_{40} + \nu_{43}$
1692.0	0.012	1693.5	0.006	$\nu_{43} + \nu_{45}$
1589.4	0.012	1588.0	0.026	ν_{14}
1585.2	0.043	1583.6	0.022	$\nu_{35} + \nu_{52}$
1498.9	0.624	1495.8	0.272	ν_{15}
1475.3	0.046	1475.6	0.071	$\nu_{39} + \nu_{52}$
1457.2	0.186	1452.6	0.146	ν_{17}
1441.4	0.196	1440.0	0.046	ν_{19}
1357.9	0.086	1355.3	0.100	ν_{21}
1338.1	0.036	1341.7	0.013	ν_{22}
1287.3	0.090	1282.3	0.052	ν_{26}
1251.9	0.034	1247.3	0.068	ν_{27}
1114.5	0.088	1114.7	0.057	ν_{34}
1040.1	0.048	1037.4	0.030	ν_{37}
988.0	0.063	979.7	0.023	ν_{38}
946.8	0.072	945.3	0.035	ν_{40}
860.7	0.019	856.2	0.013	ν_{44}
818.5	0.047	817.6	0.030	ν_{45}
806.3	0.174	802.1	0.065	ν_{46}
743.7	1	741.0	1	ν_{47}

Table 14 Harmonic mode descriptions and frequencies [cm^{-1}] of the IR active modes and modes involved in IR active combination bands for the identifications given in tables 12 and 13 of 1,2,3,4–tetrahydronaphthalene.

mode	freq	symm	description
ν_1	3200.2	a	quatro CH stretch
ν_2	3185.1	b	quatro CH stretch
ν_3	3165.7	a	quatro CH stretch
ν_4	3162.4	b	quatro CH stretch
ν_5	3073.0	b	dihydro CH stretch
ν_6	3070.0	a	dihydro CH stretch
ν_8	3057.9	b	dihydro CH stretch
ν_9	3025.4	b	dihydro CH stretch
ν_{10}	3020.3	a	dihydro CH stretch
ν_{11}	3006.9	a	dihydro CH stretch
ν_{12}	3006.4	b	dihydro CH stretch
ν_{13}	1649.3	b	aromatic CC stretch
ν_{14}	1622.1	a	aromatic CC stretch
ν_{15}	1525.4	a	aromatic CH in-plane bend
ν_{16}	1502.0	a	dihydro HCH bend
ν_{17}	1492.5	b	dihydro HCH bend
ν_{18}	1482.2	b	aromatic CH in-plane bend/dihydro HCH bend
ν_{19}	1478.8	b	aromatic CH in-plane bend/dihydro HCH bend
ν_{20}	1473.8	a	dihydro HCH bend
ν_{21}	1387.2	a	dihydro CH in-plane bend
ν_{22}	1373.8	a	dihydro CH in-plane bend
ν_{26}	1310.2	b	CH in-plane bend
ν_{27}	1272.9	a	dihydro CH in-plane bend
ν_{30}	1200.8	b	aromatic CC in-plane bend
ν_{34}	1134.3	b	quatro CH in-plane bend
ν_{35}	1100.5	a	alaphatic CC out-of-plane bend
ν_{37}	1056.1	a	ring breathe
ν_{38}	995.3	b	CC in-plane bend
ν_{39}	988.3	a	quatro CH out-of-plane bend
ν_{40}	961.5	b	quatro CH out-of-plane bend
ν_{43}	880.5	a	CH out-of-plane bend
ν_{44}	872.7	a	alaphatic CC in-plane stretch
ν_{45}	829.4	a	alaphatic CC out-of-plane bend
ν_{46}	811.9	b	CC in-plane bend
ν_{47}	753.6	b	quatro CH out-of-plane bend
ν_{52}	512.6	a	CH out-of-plane bend

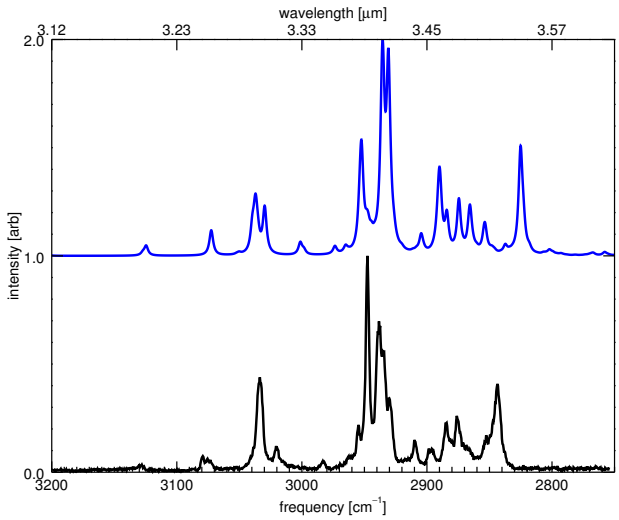

Fig. 11 Theoretical anharmonic IR spectrum of this work of 1,2,3,6,7,8–hexahydropyrene compared with the high–resolution gas–phase IR absorption spectrum of this work.

Table 15 Line positions [cm^{-1}], relative intensities, resonance components, and intensity origins for the bands of 1,2,3,6,7,8–hexahydropyrene determined from the high–resolution gas–phase IR absorption spectra and the theoretical anharmonic spectrum of this work (figure 11).

exp[1]	rel I[1]	anharm	rel I	components	I source
3128.0	0.04	3124.6	0.05	$\nu_{17}+\nu_{29}$	ν_2
3079.2	0.07				
3075.5	0.06	3072.4	0.12	$\nu_{19}+\nu_{23}$, ν_2	ν_2
3033.6	0.44	3037.1	0.29	$\nu_{17}+\nu_{26}$, ν_2	ν_2
3020.6	0.12	3029.8	0.23	$\nu_{19}+\nu_{27}$, ν_2	ν_2
2982.3	0.05	3001.2	0.07	$\nu_{18}+\nu_{29}$	ν_2
2954.8	0.22				
2947.5	1	2952.4	0.54	$\nu_{21}+\nu_{22}$, ν_8, ν_{12}	ν_8, ν_{12}, ν_6
2938.3	0.70	2935.1	0.47	ν_9, $\nu_{19}+\nu_{33}$	ν_9
		2935.8	0.40	ν_8, ν_6	ν_8, ν_6
		2936.0	0.13	$\nu_{18}+\nu_{35}$, ν_7, $\nu_{19}+\nu_{32}$	ν_7, ν_5, ν_{11}
2934.7	0.56	2931.0	0.96	ν_5	ν_5, ν_{11}
2930.1	0.34	2930.7	-	ν_6	ν_6
2910.1	0.15	2904.6	0.10	$\nu_{21}+\nu_{24}$, $\nu_{21}+\nu_{22}$, $\nu_{22}+\nu_{25}$	ν_8
2896.0	0.10	2890.0	0.41	$\nu_{21}+\nu_{26}$, ν_9	ν_9
2884.3	0.20	2884.2	0.21	$\nu_{24}+\nu_{27}$, $\nu_{25}+\nu_{26}$, ν_{16}, ν_9	ν_9, ν_{16}
2876.1	0.26	2875.4	0.27	$\nu_{26}+\nu_{26}$, $\nu_{27}+\nu_{27}$, ν_{13}	ν_{13}
				$\nu_{26}+\nu_{27}$, ν_{14}	ν_{14}
2852.7	0.17	2853.8	0.16	$\nu_{22}+\nu_{29}$, $\nu_{20}+\nu_{34}$, ν_{11}	ν_{11}
2843.7	0.40	2825.1	0.51	ν_{14}, $\nu_{26}+\nu_{27}$	ν_{14}
				ν_{13}, $\nu_{18}+\nu_{42}$	ν_{13}

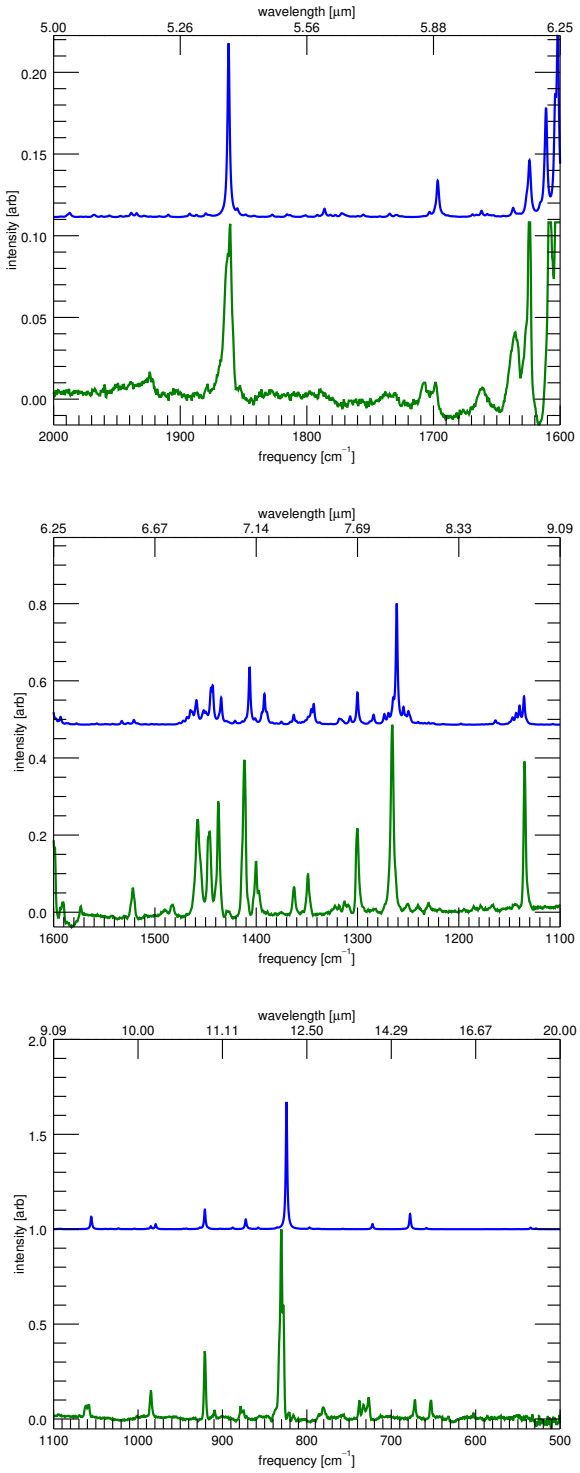

Fig. 12 The matrix–isolation infrared spectrum[2,3] of 1,2,3,6,7,8–hexahydropyrene (green, bottom of each panel) compared to the convolved (FWHM 2 cm^{-1}) theoretical anharmonic calculations of this work (blue, top each panel). Three spectral ranges are shown, with each range normalized to the local maximum to enhance details.

Table 16 Line positions [cm^{-1}], relative intensities, and vibrational mode identifications for the bands of 1,2,3,6,7,8–hexahydropyrene determined from the matrix isolation spectra and the theoretical anharmonic spectrum of this work (figure 12).

exp[2,3]	rel I	anharm	rel I	mode
1862.1	0.110	1861.8	0.106	$\nu_{57} + \nu_{56}$
1706.4	0.018	1703.1	0.003	$\nu_{57} + \nu_{66}$
1698.2	0.015	1696.7	0.022	$\nu_{62} + \nu_{64}$
1660.7	0.019	1662.1	0.004	$\nu_{64} + \nu_{67}$
1636.0	0.060	1637.1	0.006	$\nu_{56} + \nu_{69}$
1521.8	0.078	1520.7	0.013	ν_{20}
1482.9	0.032	-		
1457.5	0.260	1459.0	0.064	ν_{22}
1446.4	0.249	1444.6	0.096	$\nu_{31} + \nu_{89}$
1437.3	0.310	1434.6	0.071	ν_{26}
1411.8	0.446	1406.6	0.150	ν_{29}
1399.9	0.123	1391.9	0.080	$\nu_{65} + \nu_{72}$
1362.7	0.076	1363.0	0.026	ν_{30}
1348.9	0.105	1345.6	0.054	ν_{32}
1322.2	0.015	1318.1	0.016	$\nu_{58} + \nu_{81}$
1311.6	0.024	1307.3	0.022	$\nu_{55} + \nu_{83}$
1300.1	0.246	1300.1	0.084	ν_{37}
1265.8	0.517	1261.3	0.315	ν_{38}
1250.9	0.020	1254.6	0.047	$\nu_{49} + \nu_{88}$
1240.3	0.015	1249.8	0.036	$\nu_{44} + \nu_{90}$
1229.9	0.021	-		
1135.0	0.419	1135.6	0.074	ν_{48}
1060.2	0.077	1055.4	0.066	ν_{52}
984.8	0.157	979.1	0.026	ν_{55}
920.8	0.406	920.9	0.103	ν_{58}
909.4	0.044	-		
877.0	0.052	872.4	0.051	ν_{61}
830.1	1	824.1	0.671	ν_{64}
780.5	0.058	-		
731.1	0.068	722.2	0.027	ν_{68}
672.1	0.104	677.7	0.080	ν_{70}
653.1	0.114	658.3	0.006	$\nu_{74} + \nu_{88}$

Table 17 Harmonic mode descriptions and frequencies [cm^{-1}] of the IR active modes and modes involved in IR active combination bands for the identifications given in tables 15 and 16 of 1,2,3,6,7,8–hexahydropyrene.

mode	freq	symm	description
ν_2	3177.8	b_1	duo CH stretch
ν_4	3161.5	b_2	duo CH stretch
ν_5	3077.5	a_1	dihydro CH stretch
ν_6	3077.3	b_2	dihydro CH stretch
ν_7	3068.3	b_2	dihydro CH stretch
ν_8	3067.9	b_2	dihydro CH stretch
ν_9	3065.9	b_1	dihydro CH stretch
ν_{11}	3032.8	a_1	dihydro CH stretch
ν_{12}	3032.7	b_2	dihydro CH stretch
ν_{13}	3000.9	a_1	dihydro CH stretch
ν_{14}	3000.8	b_2	dihydro CH stretch
ν_{16}	2998.9	b_1	dihydro CH stretch
ν_{17}	1644.0	a_2	aromatic CC stretch
ν_{18}	1643.7	a_1	aromatic CC stretch
ν_{19}	1638.8	b_2	aromatic CC stretch
ν_{20}	1557.9	b_1	aromatic CC stretch
ν_{21}	1496.4	a_1	dihydro HCH bend
ν_{22}	1496.3	b_2	dihydro HCH bend
ν_{23}	1495.6	a_2	CH in-plane bend
ν_{24}	1485.8	b_2	dihydro HCH bend
ν_{25}	1484.7	a_1	dihydro HCH bend
ν_{26}	1473.4	b_1	dihydro HCH bend
ν_{27}	1471.3	a_2	dihydro HCH bend
ν_{29}	1430.2	b_2	dihydro CH in-plane bend
ν_{30}	1392.4	b_1	duo CH in-plane bend
ν_{31}	1386.4	a_1	CC in-plane stretch
ν_{32}	1376.7	b_2	CH in-plane bend
ν_{33}	1372.3	a_2	dihydro CH in-plane bend
ν_{37}	1331.3	b_1	dihydro CH in-plane bend
ν_{38}	1288.2	b_2	CH in-plane bend
ν_{42}	1249.1	b_2	CH in-plane bend
ν_{44}	1195.4	b_1	dihydro CH in-plane bend
ν_{48}	1156.2	b_1	CH in-plane bend
ν_{49}	1150.0	a_2	CC in-plane bend
ν_{52}	1076.1	b_2	alaphatic CC out-of-plane bend
ν_{55}	995.4	b_2	alaphatic CC in-plane bend
ν_{56}	949.6	b_2	duo CH out-of-plane bend
ν_{57}	947.5	a_2	duo CH out-of-plane bend
ν_{58}	935.4	b_1	CC in-plane bend
ν_{61}	886.6	a_1	dihydro CH out-of-plane bend
ν_{62}	883.4	b_1	CH out-of-plane bend
ν_{64}	841.0	a_1	dihydro CH out-of-plane bend
ν_{65}	832.3	b_2	CC in-plane bend
ν_{66}	812.4	b_1	CH out-of-plane bend
ν_{67}	808.5	b_2	CC out-of-plane bend
ν_{68}	730.6	b_2	CC in-plane bend
ν_{69}	714.5	a_2	CC in-plane bend
ν_{70}	686.4	a_1	CC out-of-plane bend
ν_{72}	586.4	a_1	body breathe
ν_{74}	543.3	b_1	CC in-plane bend
ν_{81}	399.7	a_1	body stretch
ν_{83}	332.9	a_2	CC out-of-plane bend
ν_{88}	131.2	b_1	body twist
ν_{89}	97.7	a_1	out-of plane body bend
ν_{90}	86.9	a_2	body twist

References

1 E. Maltseva, A. Petrignani, A. Candian, C. J. Mackie, X. Huang, T. J. Lee, A. G. Tielens, J. Oomens and W. J. Buma, *Submitted*, 2017.

2 D. M. Hudgins and S. A. Sandford, *J. Phys. Chem. A*, 1998, **102**, 329–343.

3 C. Boersma, C. W. Bauschlicher, Jr., A. Ricca, A. L. Mattioda, J. Cami, E. Peeters, F. Sánchez de Armas, G. Puerta Saborido, D. M. Hudgins and L. J. Allamandola, *Astrophys. J.*, 2014, **211**, 8.